Life Sciences 216 (2019) 10–21

Contents lists available at ScienceDirect

Life Sciences

journal homepage: www.elsevier.com/locate/lifescie

Intestinal luminal content from high-fat-fed prediabetic mice changes epithelial barrier function *in vitro*

R.B. Oliveira, L.P. Canuto, C.B. Collares-Buzato*

Department of Biochemistry and Tissue Biology, Institute of Biology, University of Campinas (UNICAMP), Campinas, SP, Brazil

ARTICLE INFO

Keywords:
Tight junction
Type 2 diabetes mellitus
Intestinal paracellular barrier
Caco-2 cells
Obesity

ABSTRACT

Aims: Evidence suggests that administration of a high-fat diet (HFD) results in changes in the intestinal lumen environment. Gut dysbiosis associated with intestinal barrier disruption may be involved in type 2 diabetes mellitus (T2DM) development through increased intestinal permeability, which would trigger an inflammatory response leading to peripheral insulin resistance state and ultimately T2DM. In this study, we investigated the effect of the intestinal luminal content isolated from control or HFD-fed prediabetic mice upon the tight junction (TJ)-mediated epithelial barrier in Caco-2 and MDCK epithelial cell lines.

Methods/key findings: Exposure to small intestine luminal content (SI) isolated from HFD-fed prediabetic mice induced a more significant decrease in transepithelial electrical resistance (TEER), associated with higher paracellular flux in Caco-2 and MDCK cells after 6 h and 4 h respectively, as compared to the SI obtained from control mice. Such changes were accompanied by a significant decrease in TJ content of claudins, occludin, and ZO-1, indicative of disruption of the TJ barrier. Meanwhile, large intestine luminal content from control (Ctrl-LI) and prediabetic (HFD-LI) animals did not change TEER significantly, however, paracellular flux was significantly increased after 24 h, accompanied by a decrease in ZO-1 (after HFD-LI exposure) in Caco-2 and significant changes in the junctional distribution of claudins-1, -2, occludin and ZO-1 proteins in MDCK, particularly after HFD-LI exposure.

Significance: Luminal components of intestinal content, altered by HFD exposure, induce impairment of the TJ structure and function *in vitro*, corroborating the idea of a role of the intestinal paracellular barrier in the obesity-related T2DM pathogenesis.

1. Introduction

The incidence of diabetes mellitus and obesity has increased steadily in the last thirty years [1]. Both disorders have become a health problem worldwide and are related to the modern stressful lifestyle, sedentary habits and the ingestion of fat-enriched western-type diet. Type 2 diabetes mellitus (T2DM), that corresponds to over 90% of the diabetes cases, has usually a late onset in adulthood and is clinically characterized by a moderate hyperglycemia, a chronic low-grade inflammatory state associated with peripheral insulin resistance, which is partially compensated by beta-cell hyperplasia and insulin hypersecretion [2,3]. In later stages of T2DM, there is a slow and gradual loss of beta-cell mass and function leading to a chronic hyperglycemia state, which then requires exogenous insulin administration in order to maintain normal blood glucose levels [4,5].

The pathogenesis of the T2DM is not completely understood. Recently, it has been proposed that an intestinal dysbiosis associated with intestinal barrier disruption may play a role in T2DM development [6,7]. According to this hypothesis, an impaired microbiota is linked to a higher intestinal permeability and endotoxemia (due to the increased plasma LPS levels) that may lead to insulin resistance and finally to hyperglycemia [8–10].

The intestinal barrier is well known to act as a defense mechanism against pathogen/toxin entry to the interior milieu. This barrier is composed of the intestinal epithelium itself as well as of antimicrobial peptides, immunoglobulins, and mucus secreted by the Paneth cells, immune and goblet cells, respectively. At the cell level, the intestinal paracellular barrier is constituted by the tight junction (TJ), a multiprotein complex that binds adjacent cells together and regulates the passive diffusion of substances through the intercellular space [11–13]. The transmembrane TJ-associated proteins, *i.e.* claudins and occludin, maintain cell-cell contact, cell polarization and regulate the

* Corresponding author at: Department of Biochemistry and Tissue Biology, Institute of Biology, University of Campinas – UNICAMP, CEP 13083-970 Campinas, São Paulo, Brazil.
E-mail address: collares@unicamp.br (C.B. Collares-Buzato).

https://doi.org/10.1016/j.lfs.2018.11.012
Received 16 August 2018; Received in revised form 29 October 2018; Accepted 5 November 2018
Available online 07 November 2018
0024-3205/

paracellular permeability. Intracellularly, claudins and occludin interact with cytoplasmic proteins (such as ZO-1, ZO-2, ZO-3, cingulin, 7H6 antigen, symplekin, *etc.*) that constitute the tight junctional plaque, which anchors the TJ multiprotein complex to the actin filaments [13,14]. When the TJ is disrupted, experimentally or pathophysiologically, the intestinal permeability increases and may lead to translocation of toxins and microorganisms from the luminal space into the bloodstream [8,10].

High-fat diet seems to play an important role in the modulation of the intestinal lumen environment, by shifting the gut microbiota population and increasing bile acid secretion [15–17]. These alterations of the intestinal lumen composition, including components of high caloric high-fat diet [8,15,17–19], could potentially lead to an increase in intestinal permeability, which in turn would trigger a local and systemic inflammatory response and ultimately lead to a peripheral insulin resistance state [8,9,15,20,21]. Alternatively, the increased intestinal permeability could be secondary to the locally released pro-inflammatory cytokines by an activated gut-associated lymphoid tissue and/or to dyslipidemia [19], hyperglycemia [18], and the overall inflammatory condition [9,10,15,16,22–25] associated to the diabetic state. It has been demonstrated, in different animal models of T2DM, that the increased intestinal permeability is accompanied by a reduction in the expression of some TJ proteins (*i.e.* claudins, occludin, ZO-1) in intestinal epithelia [9,16,17]. Recently, we have also shown that treatment with a high-fat diet induces a significant decrease in the junctional content of claudin-1 in intestinal epithelia indicative of disruption of the intestinal paracellular barrier during experimental type 2 prediabetes, which was reversed by butyrate diet supplementation in mice [26]. Taking into consideration the possible link between changes in the intestine environment and obesity-associated T2DM onset, we investigated in this study whether exposure to the intestine luminal content of prediabetic mice could directly induce changes in the TJ-mediated epithelial barrier *in vitro*. For that, C57BL/6J mice were chosen as an animal model of T2DM since, when challenged with a high-fat diet, they develop prediabetes after only 60 days [27]. As a model of the epithelial intestinal barrier, we have used the human colorectal adenocarcinoma cell line Caco-2, which is vastly employed *in vitro* intestinal toxicology studies since it displays many physiological and morphological features of mature enterocytes [28]. Additionally, the Madin-Darby canine kidney (MDCK) cell line was also employed in this study, a well-known epithelial barrier model [29–31], to investigate the generality of the phenomenon.

2. Material and methods

2.1. Cell culture and seeding

Caco-2 and MDCK cells were grown in 75 cm^2 plastic flasks (Nest Biotech Co. Ltd., China). Caco-2 cells were cultured in Dulbecco's Modified Eagle Medium (high glucose) (DMEM) supplemented with 10% fetal bovine serum, 2% non-essential amino acids, 1% L-glutamine and 60 mg/L gentamicin, while MDCK were cultured with Minimum Essential Medium (MEM) supplemented with 10% fetal bovine serum and 100 IU of penicillin/mL and 100 μg of streptomycin/mL (Cultilab – Campinas, Brazil) at 37 °C in a 5% CO_2 humidified incubator (Incusafe Sanyo MCO-17A, Sanyo Electric Ltd., Japan). Culture medium was changed every two days, and cells were passaged weekly. Cells were seeded on 12 mm or 30 mm diameter porous membrane cell culture inserts (Millicell, Merck Millipore, Germany), coated with collagen extracted from Wistar rats tails [32], at the density of 5.0×10^5 cells/cm^2 (MDCK) or 1.5×10^4 cells/cm^2 (Caco-2). When fully confluent (in the case of MDCK, 3–4 days after seeding, while Caco-2, after 10–11 days after seeding), monolayers were exposed at both sides (apical + basal) to the luminal content of small intestine or of the large intestine from mice of the different experimental groups.

2.2. Monolayer exposure to intestinal luminal content from normal and prediabetic mice

Male C57BL/6JUnib mice, obtained from the Multidisciplinary Center for Biological Investigation on Laboratory Animal Science (CEMIB) of the University of Campinas (UNICAMP, Brazil), were housed at 22–25 °C on a 12 h light/12 h dark cycle and had access to water and food *ad libitum*. Between the age of 16 to 20 weeks, mice were fed a standard chow diet (content in 100 g: 4.5 g lipids, 53 g carbohydrates and 23 g proteins) (Nuvital CR1, Colombo, Paraná, Brazil) or a high-fat diet (HFD) (content in 100 g: 21 g lipids, 50 g carbohydrates and 20 g proteins) for 60 days. After this period, control and HFD-fed mice were weighed, had the glycemia measured and euthanized in a CO_2 chamber after a 12 h-fasting period, as previously described [27]. Small and large intestines were removed at sterile conditions (inside the laminar flow hood) and the luminal content washed with a total of 15 mL sterile Krebs-bicarbonate buffer (concentration in mM: NaCl 115, KCl 5, $MgCl_2$ 1, $CaCl_2$ 1.24, $NaHCO_3$ 1, HEPES 15; pH = 7,4 equilibrated with CO_2 5%) containing 100 mg/dL glucose. In order to uniformize the microorganism density from the small and large intestines to be applied to the cells, we have employed the Optical Density measurement method [33,34]. For that, the intestinal luminal contents were centrifuged in Falcon tubes at 2100 RCF for 1 min 30 s and the supernatant collected, read in a spectrophotometer (600 nm - PowerWave XS2, Biotek Instruments, USA) and diluted in sterile buffer (when necessary) to reach an absorbance of 0.05 (corresponding to the lowest Abs value measured in the intestinal content samples obtained). Just after isolation, Caco-2 and MDCK monolayers were exposed to the intestinal suspensions up to 24 h. All experimental protocols with the animals were approved by the Ethics Committee on Animal Use (CEUA) of UNICAMP under protocol #3040-1.

2.3. Transepithelial electrical resistance (TEER) and paracellular flux measurements

TEER was evaluated across cell monolayers grown on 12 mm inserts using two Ag/AgCl 'chopstick' electrodes coupled to a combined voltmeter and constant current source (EVOM, World Precision Instruments, UK) up to 24 h after intestinal luminal content exposure. The final TEER was calculated as follows: blank membrane insert resistance (without cells) was measured in every experiment and subtracted from the raw TEER value of the monolayer and, then, multiplied by the membrane area (1.13 cm^2) to give the final TEER value ($\Omega \cdot cm^2$). The average of the TEER displayed by the monolayers was: 456.6 ± 19.4 $\Omega \cdot cm^2$ (n = 89) for Caco-2 and 691.9 ± 26.3 $\Omega \cdot cm^2$ (n = 95) for MDCK cells. The TEER data was expressed as a percentage in relation to the initial mean value (at 0 h, before luminal content exposure) [18].

The transepithelial flux was assessed using the nonabsorbed, paracellular markers, Phenol Red (MW 357 kDa) (Sigma) and Lucifer Yellow (LY) (MW 457.25 kDa) [18,30]. Caco-2 and MDCK cells, grown on 30 mm permeable cell culture inserts, were transferred to a new plate containing luminal content wash from the small or large intestines, or Krebs solution, where Phenol red (100 μM) or Lucifer Yellow (100 μM) was added to, whereas the apical medium was replaced with the same basal solution without the marker. After the incubation period, triplicates of 0.2 mL samples were taken from the apical and basolateral solutions and read at 492 nm in a microplate reader (Biotek Instruments, PowerWave XS2, USA) for the Phenol Red flux, or read at 428 nm (excitation wavelength) and 535 nm (emission wavelength) using the Synergy H1 microplate reader (Biotek Instruments, USA) for the LY flux. The transepithelial flux (Ft) of both paracellular markers, taken as an index of paracellular permeability, was calculated as:

$$Ft = Abs_a \times 100/Abs_a + Abs_b$$

where Abs_a is the Absorbance of the apical solution and Abs_b is the Absorbance of the basal solution.

2.4. Immunocytochemistry for junctional proteins

Caco-2 and MDCK cell monolayers were fixed and kept in −20 °C methanol until the indirect immunofluorescence reaction. After washing with phosphate buffered saline (PBS - 0.05 M, pH = 7.4), the monolayers were incubated with 3% fetal bovine serum (FBS) in PBS for 30 min at room temperature (RT) and then incubated with primary antibodies (diluted in PBS plus 3% FBS – raised against claudins-1, -2, occludin and ZO-1) (Table I; Supplementary material) overnight at 4 °C. For occludin and ZO-1 detection, cells were treated with 0.1% Triton x-100 in PBS for 10 min prior to antibody incubation. Subsequently, monolayers were incubated for 1 h with the specific FITC-conjugated secondary antibody (Sigma) and DAPI (Sigma, cat number D9542) (dilution 1:1000 in PBS plus 3% FBS) at RT. Monolayers were then washed several times with PBS, mounted with Vectashield (Vector Laboratories) and analyzed in the same microscopic session, using the same illumination/contrast parameters in order to compare fluorescence between treated and control groups (Leica TCS SP5 II microscope or Observer Z1 microscope, Zeiss). The fluorescence degree for all the junctional proteins studied was measured using the free software Image J (http://rsbweb.nih.gov/ij/) in digital images obtained from 5 representative areas of each monolayer analyzed. Using the multi-point tool, 60 points were randomly selected at the intercellular contact in every image sampled and expressed as arbitrary fluorescence units. Claudin-2 was only analyzed in MDCK cells since it was not immunodetected in Caco-2 with the antibody employed. In the case of the analysis of claudin-1 immunoreaction, we have used a scoring system to determine the degree of alteration of cell distribution of this junctional protein in MDCK cells after exposure to large intestine content. For that, each microscopic image of claudin-1 immunofluorescence was scored as follows: score 0, normal distribution characterized by a continuous and linear labeling at the cell-cell contact region; score 1, altered distribution characterized by a discontinuous labeling at the cell-cell contact regions; score 2, altered distribution characterized by a marked decreased or absent intercellular labeling. The degree of alteration to the claudin-1 junctional distribution in the MDCK cells was determined by calculating the score mean value for each experimental group according to this classification.

2.5. Western Blot for junctional proteins

Caco-2 and MDCK monolayers were scraped from 30 mm inserts and homogenized in an anti-protease cocktail (composition: 10 mM imidazole pH 7.4; 4 mM EDTA; 1 mM EGTA; 200 μM DTT; 0.5 μg/mL pepstatin A; 200 KIU/mL aprotinin; 200 μM phenylmethylsulfonyl fluoride; 2.5 μg/mL leupeptin e 30 μg/mL trypsin inhibitors). An equal amount of proteins (20 μg) was mixed with 5× concentrated Laemmli sample buffer (30% of the aliquot volume) and separated by electrophoresis in 6.5% or 12% polyacrylamide gels, transferred onto nitrocellulose membranes (Bio-Rad) and stained with Ponceau S solution (Sigma) for checking the membrane transfer efficiency. Membranes were blocked with 5% dry skimmed milk, incubated with primary antibody to different tight junction proteins (claudins-1, -2, occludin and ZO-1) (Table I; Supplementary material) followed by incubation with specific secondary antibody conjugated with horseradish peroxidase (HRP), rinsed and the signal was developed by an enhanced chemiluminescence kit (SuperSignal West Pico Chemiluminescent Substrate, Thermo Fisher Scientific). Membrane images were acquired using the G:box system (Syngene - UK), band signals were quantified by optical densitometry (Image J) and then the membranes were reprobed using an anti-beta-actin as a loading control. Finally, optical densitometry values were expressed as a ratio of specific tight junction protein/beta-actin signal.

2.6. Cell viability

Cell viability was evaluated by the neutral red uptake assay [30]. Caco-2 and MDCK cells were seeded in 96-well plates; when fully confluent, the monolayers were exposed to luminal content from the small or large intestines of normal or prediabetic mice, or to Krebs solution for up to 24 h. Subsequently, cells were incubated with neutral red dye (40 μg/mL in Krebs solution) for 3 h at 37 °C; then, they were fixed with 4% formaldehyde solution containing 1% calcium chloride and the stain solubilized in 1% acetic ethanol for 15 min at 37 °C. Finally, the absorbance was measured at 570 nm using a microplate reader (PowerWave XS2), and the cell viability was expressed as the percentage in relation to the mean of absorbance values of the Krebs solution-exposed monolayers (taken as 100%).

2.7. Statistical analyses

Statistical analyses were performed using the GraphPad Prism, version 5.00 for Windows (GraphPad Software, La Jolla, CA, USA). For numerical results, data were expressed as the means ± standard error of the mean (SEM). For multiple comparisons among experimental groups, we have used the One or Two-way analysis of variance (ANOVA) followed by the Bonferroni's post-test. For the metabolic parameters of mice, statistical significance was assessed using Student's *t*-test (two-tailed). The statistical significance level was set at $P < 0.05$.

3. Results

In order to confirm the prediabetic state in our animal model, we have measured the weight gain, fasting and postprandial glycemia, before collecting the intestinal luminal content. As expected, high-fat diet (HFD)-fed mice displayed a significant body weight gain (Ctrl 31.82 ± 0.67 (17) *vs.* HFD 41.89 ± 1.19 (17) grams, $P < 0.0001$), a postprandial hyperglycemia (Ctrl 140.8 ± 2.30 (6) *vs.* HFD 181.8 ± 12.94 (5) mg/dL, $P < 0.001$) associated with increased fasting glycemia (Ctrl 79.62 ± 3.22 (13) *vs.* HFD 96.08 ± 5.67 (12) mg/dL, $P < 0.05$). These alterations are in accordance with our previous work [27,35] that indicates, in conjunction with other metabolic parameters, the development of obesity and prediabetes in C57 mice after 60 days of treatment with the HFD.

Exposure to small intestine luminal content (SI) from these HFD-fed prediabetic mice (HFD-SI) induced a significant time-dependent decrease in the TEER, starting from 4 h after exposure ($P < 0.001$) in Caco-2 monolayers, as compared to the control counterparts exposed to SI from normal mice (Ctrl-SI) and that exposed to Krebs buffer only (Krebs-Ctrl) ($P < 0.05$, Fig. 1a). When compared to Krebs-exposed Caco-2 cells, those exposed to SI content from normal mice (Ctrl-SI) also induced a reduction in TEER that was comparatively less pronounced than that induced by SI from prediabetic mice (HFD-SI) (Fig. 1a). The epithelial paracellular permeability (Pp) assay showed that this TEER decrease was accompanied by a significant increase in the basal-to-apical phenol red flux ($F_{b\rightarrow a}$) across Caco-2 monolayers exposed to HFD-SI and Ctrl-SI at 6 h (in relation to Krebs, $P < 0.05$) and at 24 h ($P < 0.001$), which was greater in HFD-SI-treated cells in relation to Ctrl-SI-treated ones ($P < 0.01$; Fig. 1b).

As for the large intestinal luminal content (LI), exposure to either LI isolated from prediabetic (HDF-LI) or normal (Ctrl-LI) mice induced a subtle, but significant in the case of Ctrl-LI, increase in the TEER across Caco-2 monolayers as compared to Krebs-exposed monolayers (Krebs-Ctrl group) ($P < 0.01$; Fig. 1a). Surprisingly, both treatments equally increased the epithelial Pp to phenol red in Caco-2 in comparison with the Krebs-Ctrl group ($P < 0.001$; Fig. 1b). In order to check this apparent inconsistency between TEER and Pp data, we have tested another paracellular marker, the LY. The Pp to LY showed a slight increase in the transepithelial flux of this marker after Caco-2 exposure to LI for 24 h compared to Krebs, which was only significant in the case of the LI

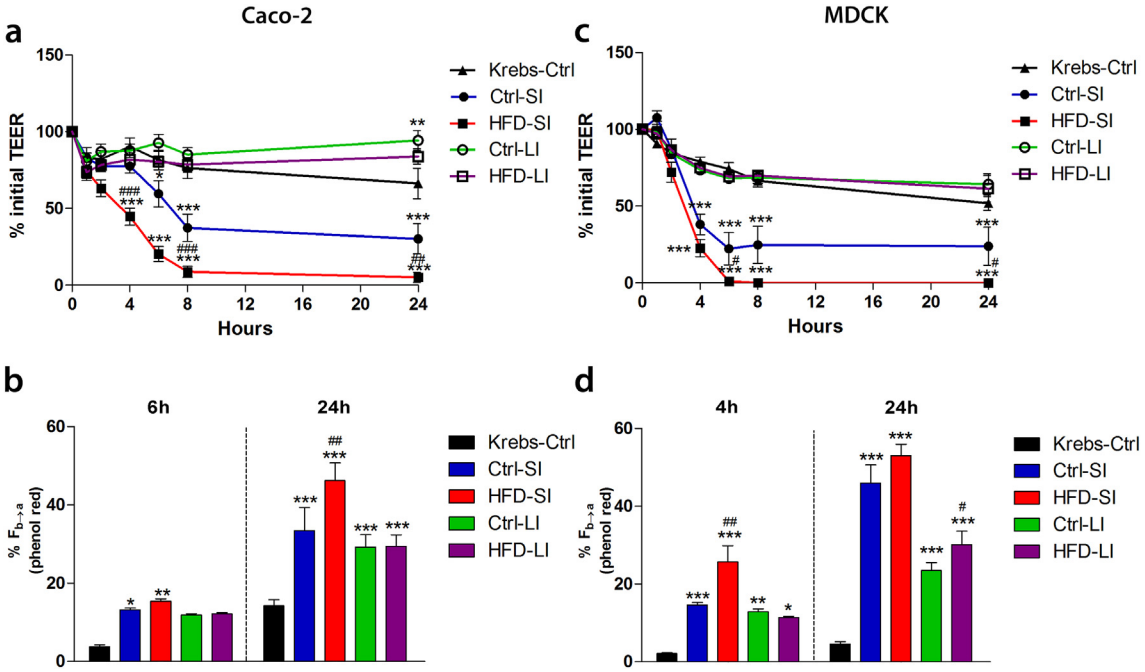

Fig. 1. Exposure to luminal content of small intestine (SI) or large intestine (LI) isolated from control (Ctrl) and high-fat-fed (HFD) prediabetic mice induced changes in the transepithelial electrical resistance (TEER) and transepithelial paracellular flux (basal to apical; $F_{b\rightarrow a}$) of phenol red in Caco-2 and MDCK monolayers. Ctrl-SI and HFD-SI induced a time-dependent decrease in TEER in both Caco-2 (a) and MDCK cell lines (c), as compared to Krebs-exposed monolayers; the reduction in the TEER was even greater after HFD-SI than that after Ctrl-SI. These changes in TEER were paralleled by an increase in epithelial paracellular permeability of the marker, phenol red (b, d). In contrast, Ctrl-LI and HFD-LI did not induce marked alteration to the TEER of Caco-2 and MDCK (a, c), however, the transepithelial flux of phenol red was significantly increased after 24 h in comparison to Krebs-exposed monolayers (b, d). Initial TEER mean value (0 h, before luminal content exposure) was taken as 100% in comparison to the followed time points measured in 15–19 monolayers from 4 to 5 independent experiments (Two-way ANOVA and Bonferroni's test). For the transepithelial flux, phenol red apical absorbance was expressed as a percentage in relation to the apical + basal absorbance (taken as 100%) of 5–14 monolayers from 2 to 5 independent experiments. *P < 0.05, **P < 0.01, ***P < 0.0001 in relation to Krebs; #P < 0.05, ##P < 0.01, ###P < 0.0001 in relation to its respective Ctrl (One-way ANOVA and Bonferroni's post-test). (For interpretation of the references to color in this figure legend, the reader is referred to the web version of this article.)

isolated from prediabetic mice (HFD-Li) (Flux apical-to-basal of LY: Krebs-Ctrl group = 13.22 ± 1.10% (5); Ctrl-LI = 15.24 ± 2.07% (5); HFD-LI = 18.76 ± 1.19% (5)*; *P < 0.05 Krebs-Ctrl *vs.* HFD-LI; *t*-Student, two-tailed).

Similar results were obtained with MDCK cells, although in general, this cell line displayed a higher sensitivity to exposure to intestinal content than Caco-2. The TEER measurement showed that both Ctrl-SI and HFD-SI exposure reduced significantly this parameter from 4 h up to 24 h of treatment (P < 0.001) in relation to Krebs-Ctrl monolayers (Fig. 1c). In addition, TEER values in HFD-SI-exposed MDCK cells were significantly lower than the Ctrl-SI ones, reaching nearly zero value after 6–8 h of treatment (Fig. 1c), which was associated with an increased epithelial Pp at 4 h (P < 0.001 in relation to Krebs and P < 0.01 in relation to Ctrl-SI; Fig. 1d), and being markedly enhanced after 24 h (P < 0.001 in relation to Krebs). As in Caco-2 cells, Ctrl-LI and HFD-LI exposure induced a tendency of increase in TEER across MDCK monolayer (Fig. 1c), which was accompanied by a significant increase in epithelial Pp to phenol red already observed at 4 h (P < 0.05; Fig. 1d), which was even greater after 24 h, specially in the case of treatment with HFD-LI (P < 0.001 in relation to Krebs; P < 0.05 in relation to Ctrl-LI). This finding was confirmed by the LY flux assay that showed a tendency of increase in paracellular permeability after exposure of MDCK monolayers to HFD-LI in comparison to those treated with Ctrl-LI or exposed to Krebs only (apical-to-basal flux of LY: Krebs-Ctrl group = 7.88 ± 0.21% (5); Ctrl-LI = 8.03 ± 0.13% (5); HFD-LI = 9.11 ± 0.53% (5)*; *P = 0.076 Ctrl-LI *vs.* HFD-LI; *t*-Student, two-tailed).

As seen in Fig. 1a and c, Ctrl-SI and HFD-SI induced a marked decrease in TEER in both Caco-2 and MDCK cells after 6 h and 4 h respectively, that may suggest a cytotoxicity and/or impairment of cell adhesion after exposure to intestinal luminal content. In order to investigate this possibility, cell viability was assessed by the neutral red uptake assay and cell morphology analyzed by phase contrast microscopy (Fig. 2). The neutral red absorbance showed that the short-term exposure to all experimental conditions tested induced no significant changes in cell viability in Caco-2 cells (at 6 h, Fig. 2f) or MDCK cells (at 4 h, Fig. 2r), while HFD-SI exposure resulted in changes in cell morphology from a typical polyhedral shape to a globular or fusiform morphology in Caco-2 (Fig. 2c) and MDCK cells (Fig. 2o), respectively. In contrast, a more prolonged exposure (24 h) to intestinal luminal content led to an overall reduction in cell viability in both cell lines, although MDCK cells seemed to be more affected than Caco-2 cells (*i.e.*, after SI exposure, the cell viability was < 4% in MDCK cells while Caco-2 cells displayed a viability around 35–60%). In addition, the deleterious effect of SI exposure on cell viability was more pronounced than that seen after LI, while HFD-SI (P < 0.0001 in Caco-2 and MDCK) and HFD-LI treatment (P < 0.01 in Caco-2; P < 0.0001 MDCK cells) resulted in a lower cell viability index in comparison with their respective controls, Ctrl-SI and Ctrl-LI, especially in the case of MDCK cell line. The decrease in cell viability after 24 h exposure to Ctrl-SI and HFD-SI was associated with some cell loss in Caco-2 (Fig. 2h,i) or with a complete cell detachment from the substrate in the case of MDCK cells (Fig. 2t,u). Meanwhile, after 24 h, only HFD-LI induced some cell loss in both Caco-2 and MDCK monolayers.

In order to assess the changes in TJ structure after intestinal content exposure, monolayers were immunolabeled for some junctional proteins (claudins-1 and 2, occludin, and ZO-1) and the junctional content was determined by a semi-quantitative analysis. Since we observed, as described above, that 24 h exposure to small intestinal luminal content (SI) resulted in massive cell detachment in MDCK as well as in Caco-2

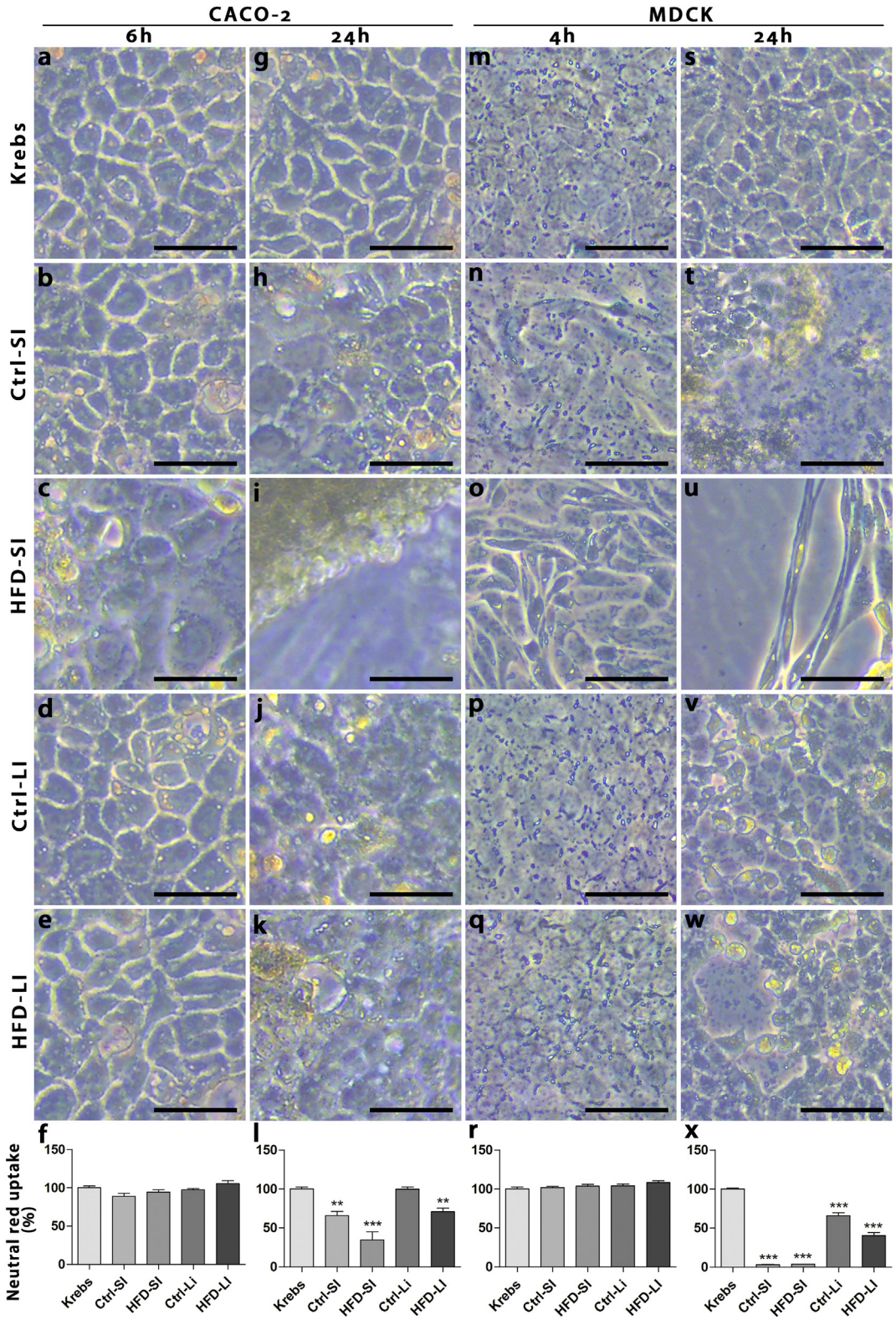

Fig. 2. Cell morphology and viability of Caco-2 and MDCK monolayers after exposure to the luminal content of small intestine (SI) or large intestine (LI) isolated from control (Ctrl) and high-fat-fed (HFD) prediabetic mice.

Cell morphology was observed by contrast-phase microscopy (a–e, g–k, m–q, s–w) and cell viability was assessed by neutral red uptake assay (f, l, r, x) after intestinal luminal content exposure. At 6 h and 4 h, Caco-2 (f) and MDCK (r) monolayers, respectively, did not show significant changes in cell viability in relation to Krebs. However, after 24 h, Ctrl-SI and HFD-SI induced decreased cell viability (l, x) and cell loss/monolayer detachment in both cell lines, that were more pronounced in MDCK (t,u) than in Caco-2 cells (h, i). At 24 h, HFD-LI induced some cell loss in both Caco-2 (k) and MDCK monolayers (w), but Ctrl-LI was only deleterious to MDCK monolayers (v). Images a–e; g–k; m–q; s–w represent Caco-2 and MDCK cell monolayers exposed to intestinal luminal contents (SI, LI) from normal (Ctrl) or prediabetic mice (HFD) or to Krebs buffer. Scale bar, 50 μm. Graphs f, l, r, and x depict neutral red uptake absorbance in treated monolayers, expressed as a percentage in relation to Krebs-exposed absorbance mean values (taken as 100%) of 9 to 24 monolayers from 2 independent experiments. **P < 0.01, ***P < 0.0001 in relation to Krebs (One-way ANOVA and Bonferroni's post-test). (For interpretation of the references to color in this figure legend, the reader is referred to the web version of this article.)

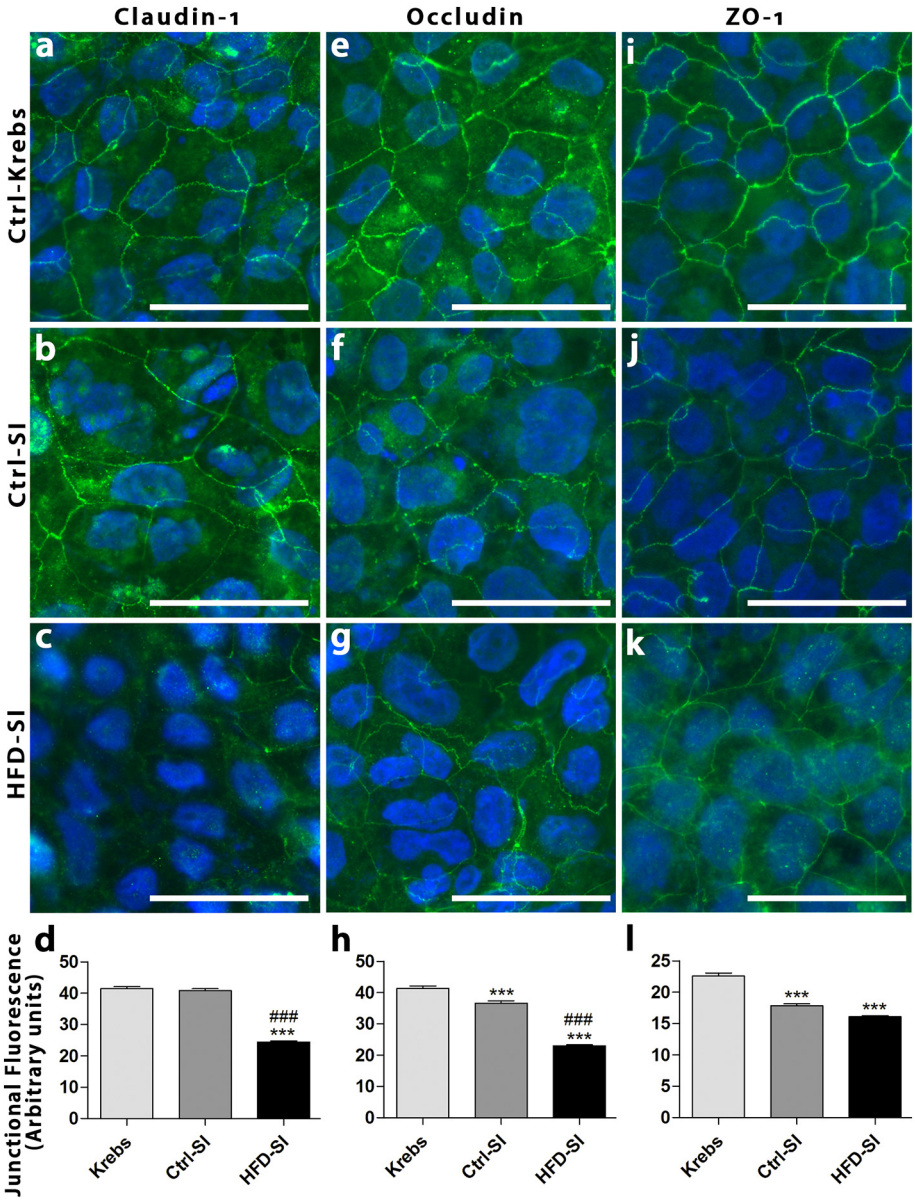

Fig. 3. Intercellular distribution and content of tight junctional proteins in Caco-2 monolayers after 6 h-exposure to the luminal content of small intestine (SI) isolated from control (Ctrl) and high fat-fed (HFD) prediabetic mice.
Images a–c, e–g, i–k display the tight junction-associated proteins evaluated by immunofluorescence in Caco-2 monolayers (immunolabeled for claudin-1, occludin, and ZO-1 in green - FITC; DAPI/nuclei in blue). The junctional fluorescence degree analysis at cell-to-cell contact showed a significant decrease in claudin-1 (d), occludin (h) and ZO-1 (l) after 6 h exposure to HFD-SI (d) in relation to Ctrl-LI and/or Krebs-exposed monolayers (n = 4–5 monolayers/group). In addition, Ctrl-SI also reduced significantly the junctional fluorescence density of occludin (h) (n = 5–6 monolayers/group) and ZO-1 (l) (n = 4–5 monolayers/group) after the same period of time in relation to Krebs. Scale bar, 50 μm. ***P < 0.0001 in relation to Krebs; ###P < 0.0001 in relation to Ctrl-SI (One-way ANOVA and Bonferroni's post-test). (For interpretation of the references to color in this figure legend, the reader is referred to the web version of this article.)

cells after HFD-SI, all the following experiments were performed at shorter time periods (at 6 h for Caco-2 and at 4 h for MDCK cells). In the case of the large intestine luminal content, the cells were exposed up to 24 h since shorter exposure did not induce significant changes in paracellular permeability, particularly in Caco-2 cells. The small intestine luminal content isolated from prediabetic mice (HFD-SI) induced a significant reduction in the junctional content of claudin-1, occludin, and ZO-1 after 6 h of Caco-2 exposure in comparison with those exposed to Krebs or to Ctrl-SI from normal mice ($P < 0.0001$ Fig. 3d, h, l). In addition, Ctrl-SI-exposed Caco-2 monolayers displayed a significant decrease in occludin and ZO-1 junctional content as compared to Krebs-exposed monolayers ($P < 0.0001$ Fig. 3h and l). As for the large intestine luminal content, both Ctrl-LI and HFD-LI induced a significant decrease in ZO-1 junctional content ($P < 0.0001$, Fig. 4l) after 24 h exposure, however, both experimental conditions did not change significantly the junctional content of claudin-1 (Fig. 4d) and occludin (Fig. 4h). Immunoblotting showed that Ctrl-SI ($P < 0.05$) and HFD-SI ($P < 0.01$) significantly reduced the total amount of occludin in Caco-2 cells (Fig. 5-b) as compared to Krebs-exposed monolayers, but did not affect the cell expression of claudin-1 (Fig. 5a) and ZO-1 (Fig. 5c). Furthermore, Ctrl-LI and HFD-LI induced no significant alteration to the total amount of TJ proteins as revealed by immunoblotting (Fig. 5d–f).

Regarding the MDCK cells, we observed a similar change in junctional content and expression of TJ proteins to that seen with Caco-2 cells after exposure to SI and LI, although MDCK monolayers seemed to display higher sensitivity to these experimental conditions than Caco-2 cells. Exposure for 4 h to small intestine luminal content (SI) from normal (Ctrl-SI) and prediabetic (HFD-SI) mice induced a marked decrease in claudin-1 (Fig. 6a–d), claudin-2 (Fig. 6e–h), and occludin (Fig. 6i–l), but only HFD-SI reduced ZO-1 junctional content (Fig. 6m–p) in relation to Krebs-exposed monolayers ($P < 0.001$). Overall, TJ protein reduction was more prominent in MDCK monolayers exposed to HFD-SI ($P < 0.0001$) in relation to Ctrl-SI, except for claudin-2 (Fig. 6e–h). Regarding the large intestine luminal contents, Ctrl-LI and HFD-LI dramatically changed claudin-1 cellular distribution after 24 h (Fig. 7a–d). The immunodetection of claudin-1 showed that the typical intercellular labeling, characterized by a continuous line at the cell-cell contact site (as seen in Krebs - Fig. 7a) was disrupted in MDCK cells after LI exposure. After 24 h-treatment, claudin-1 was internalized into the cytoplasm and the remaining protein at the intercellular site had a diffuse appearance. These observations were

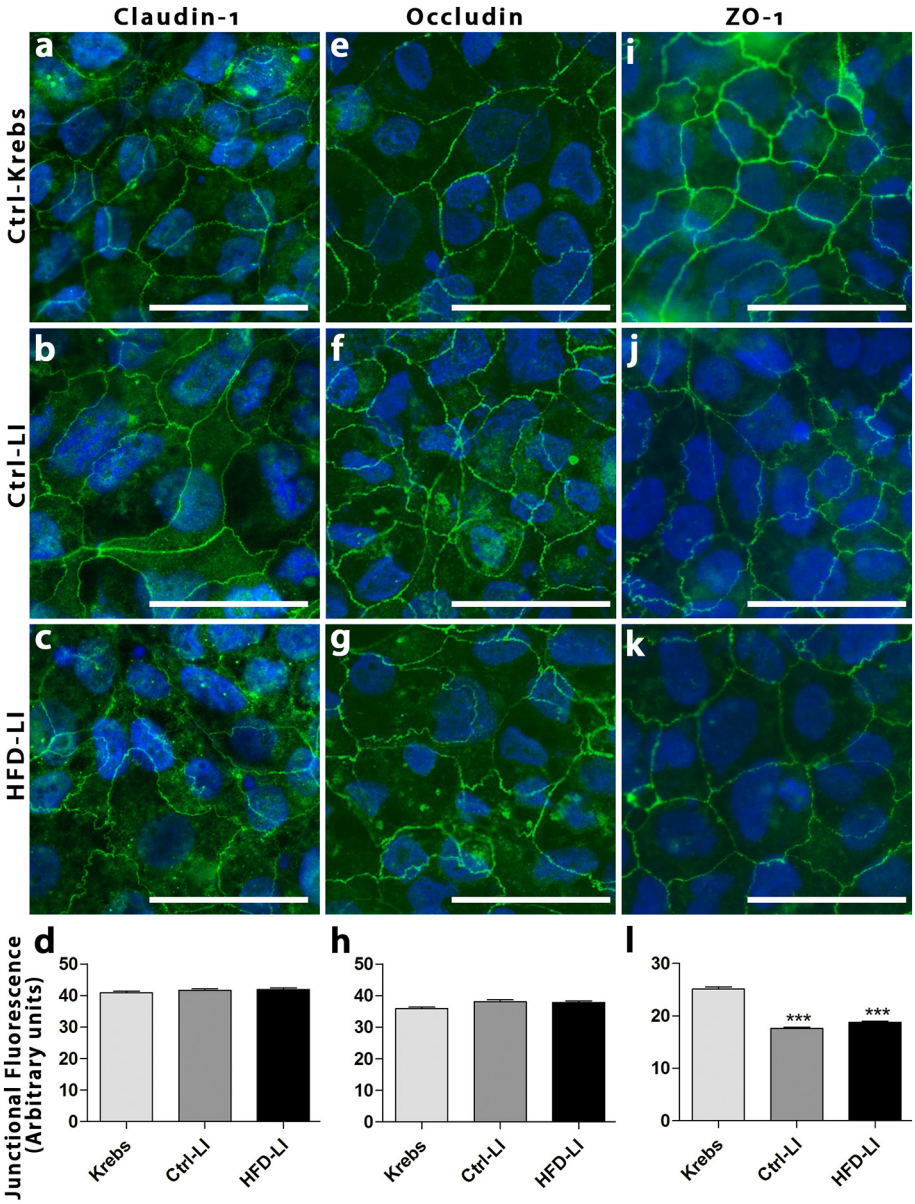

Fig. 4. Intercellular distribution and content of tight junctional proteins in Caco-2 monolayers after 24 h-exposure to the luminal content of large intestine (LI) isolated from control (Ctrl) and high-fat-fed (HFD) prediabetic mice.
Images a–c; e–g; i–k display the junctional tight junction-associated proteins evaluated by immunofluorescence in Caco-2 monolayers (immunolabeled for claudin-1, occludin, and ZO-1 in green - FITC; DAPI/nuclei in blue). The junctional fluorescence degree analysis at cell-to-cell contact showed only a significant decrease in ZO-1 after 24 h exposure to Ctrl-SI and HFD-SI (l) (n = 5 monolayers/group). However, no change was observed in the junctional fluorescence pixel density of claudin-1 (d) (n = 5 monolayers/group) and occludin (h) (n = 6 monolayers/group) after treatments in comparison with Krebs. Scale bar, 50 μm. ***P < 0.0001 in relation to Krebs (One-way ANOVA and Bonferroni's post-test). (For interpretation of the references to color in this figure legend, the reader is referred to the web version of this article.)

confirmed semi-quantitatively as shown in Fig. 7d that also revealed that these effects were even more marked after exposure to HFD-SI as compared to Ctrl-SI (Fig. 7d). As for the other TJ proteins, exposure to LI luminal content did not change the cell distribution of these proteins, although altered their junctional content as shown by a semi-quantitative analysis of the immunofluorescence images (Fig. 7). Ctrl-LI exposure for 24 h increased occludin junctional content, that displayed an altered cell distribution (Fig. 7i–l), as well as a reduced claudin-2 junctional content (Fig. 7e–h) in relation to Krebs ($P < 0.0001$). Meanwhile, HFD-LI induced a significant decrease in claudin-2 (Fig. 7e–h), occludin (Fig. 7i–l), and ZO-1 junctional content (Fig. 7m–p) in relation to Krebs and Ctrl-LI ($P < 0.0001$). Immunoblotting analysis showed that, in comparison with the Krebs-exposed monolayers, Ctrl-SI and HFD-SI exposure to MDCK cells reduced the total amount of occludin (Fig. 8c), that was relatively more pronounced after HFD-SI ($P < 0.01$) than Ctrl-SI ($P < 0.05$). Meanwhile, no significant changes in claudin-1 (Fig. 8a), claudin-2 (Fig. 8b), and ZO-1 (Fig. 8d) cell amount were seen after exposure to small intestine luminal contents either from normal or prediabetic mice. As for LI content exposure, immunoblotting revealed reduction of cellular content of all the junctional proteins analyzed (Fig. 8e–j), that was statistically significant in the case of claudin-1 (Fig. 8e), claudin-2 (Fig. 8f), and occludin (Fig. 8g), being overall even more pronounced after HFD-LI than Ctrl-LI exposure, in relation to Krebs.

4. Discussion

In this study, we investigated, using an *in vitro* system, the current idea that an impairment of the intestinal barrier can be a contributing factor in the T2DM pathogenesis and may be triggered by an agent found within the intestinal environment [7,9,17]. For that, epithelial cell lines were exposed to the intestinal content isolated from normal and prediabetic mice. We demonstrated that the *in vitro* exposure to intestinal luminal content induces cell detachment from the substrate as well as significant changes in cellular distribution and/or junctional content of several TJ proteins in Caco-2 and MDCK cells that were indicative of disruption of the epithelial barrier. These alterations were, in general, more pronounced after exposure to intestinal luminal content isolated from prediabetic mice than that from normal mice, which is in agreement with the ongoing hypothesis [17,22,25]. MDCK cells displayed a more severe response to the exposure of intestinal content than Caco-2 cells, which may be related to the intestinal origin of the

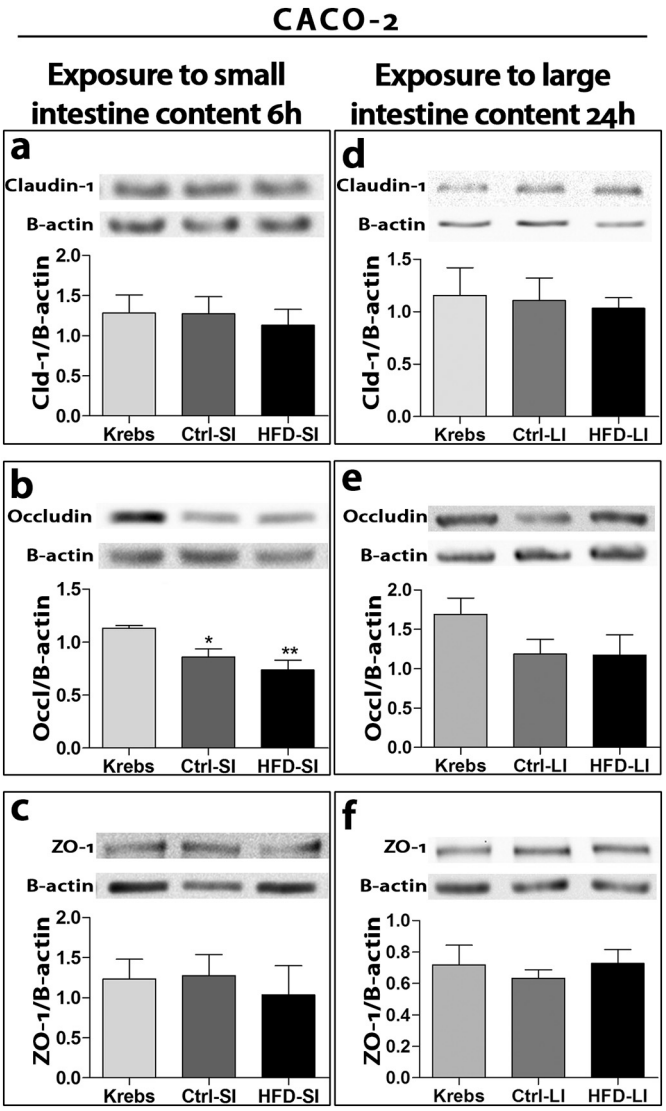

Fig. 5. Immunoblotting for junctional proteins in Caco-2 monolayers exposed to the luminal content of the small intestine (Ctrl-SI; HFD-SI) and large intestine (Ctrl-LI; HFD-LI) isolated from control (Ctrl) and high-fat-fed (HFD) mice.
The optical density analysis of the TJ-associated proteins from Caco-2 homogenates was performed in membranes obtained by Western Blotting. Exposure to small intestine content for 6 h induced a decrease in occludin cell content (b, n = 8–9/group), which was more pronounced after HFD-SI than Ctrl-SI, but no significant change in claudin-1 (a, n = 8–9 membranes/group) and ZO-1 (c, n = 8 membranes/group) cell contents in relation to Krebs-exposed cells. Exposure to large intestine content for 24 h showed no significant alteration of claudin-1 (d, n = 6/group), occludin (e, n = 6/group), and ZO-1 (f, n = 6/group) in Caco-2 monolayers. Beta-actin was employed as the loading control. Results are expressed as means ± SEM. *P < 0.05 **P < 0.01 in relation to Krebs (One-way ANOVA and Bonferroni's post-test).

latter in contrast with the renal origin of the former. In addition, exposure to small intestinal luminal content resulted in alterations to the TJ structure which were more significant than those after large intestinal luminal content.

The short-term exposure (4 to 6 h) of both epithelial cell lines to luminal content of the small intestine (SI) induced significant disruption of the epithelial paracellular barrier as revealed by the decrease in TEER and increase in transepithelial flux of a paracellular marker, that were associated with a decrease in the junctional content of TJ structural proteins such as claudin-1, occludin and ZO-1. In the case of occludin, the decrease in its junctional content occurred in parallel with a reduction in cellular expression of this protein as shown by Western Blot. In general, these alterations were more marked after exposure to HFD-SI in comparison with those from Ctrl-SI group. The claudin-1 and occludin make up the TJ strands and determine the tightness of the paracellular barrier while the ZO-1 is a known scaffold protein that plays a regulatory role of the TJ function [14,23,36]. Similar changes to that described herein, regarding the cellular distribution and expression of these proteins, have been directly related to the disruption of epithelial TJ function in other *in vitro* and *in vivo* conditions [9,16,17,30].

Besides the claudin-1, that is known as a barrier-forming claudin [12,36], we have also investigated the cell distribution and expression of the pore-forming claudin-2 in MDCK cells. Interestingly, the junctional amount of this protein was significantly reduced in Ctrl-SI-treated monolayers and, to a lesser extent, in HFD-SI-treated cells in comparison with Krebs-exposed ones, which suggests a slight strengthening of the paracellular barrier to ions by agents from the intestine lumen. A relatively higher junctional content of claudin-2 was seen after HFD-SI exposure, which is in line with the data showing a more significant reduction in TEER (a parameter that measures the ionic flux across the monolayers) observed in the HFD-SI-treated MDCK cells compared to the Ctrl-SI-treated ones. The disruption of the TJ structure seen after exposure to SI content in both cell lines was not due to a cytotoxic effect since no change in cell viability and cell attachment to the substrate was detected, by the neutral red assay, after short-term treatment (up to 6 h) with SI content. Taken all together, our data suggest that components of the small intestine lumen, especially that isolated from prediabetic mice, can directly modulate, at short-term, the TJ proteins, leading to a decrease in the paracellular barrier function, particularly to molecules, in the epithelial cell lines studied.

In contrast, a more prolonged exposure to SI content (24 h) induced a significant decrease in cell viability as well as led to cell detachment from the substrate in Caco-2 cells, but particularly in MDCK cells, which prevented further morphological analysis of these cell monolayers. This marked decrease in viability observed in our study indicates that components of the intestine luminal content were deleterious, after a relatively long-term exposure, to the cell lines tested herein. The epithelial cells themselves, as well as their TJs, are important components of the intestinal barrier along with the mucus secreted by the goblet cells and the antimicrobial agents secreted by the cells of the immune system [11,37]. However, neither Caco-2 nor MDCK cell lines are known to be mucus-secreting cells [38,39]. Therefore, the lack of a protective barrier, provided by the mucus and immune cells, can explain the direct cytotoxic effects of exposure to SI content to our *in vitro* model.

In comparison with the SI luminal content, both cell lines displayed a different response to the exposure to large intestinal luminal content (LI). First of all, the exposure to LI content for a short period (< 6 h) did not induce significant changes in epithelial barrier function neither in cell viability. Only after 24 h-exposure to Ctrl-LI or HFD-LI content, we observed a subtle increase in TEER that was, surprisingly, associated with a significant increase in the transepithelial flux of phenol red in both cell lines and, in the case of LY flux, a significantly increased epithelial permeability was seen only after HFD-LI in Caco-2 cells (a tendency in the case of MDCK cells). At the moment, we do not have a definitive explanation for the discrepancy seen between the measurements of these two parameters (TEER and flux) after cell exposure to LI content, but it seems to be consistent since was observed in both cell lines of different origins. Although the measurements of TEER and transepithelial flux are recognizable assays to evaluate the integrity of the epithelial barrier [40,41], they in fact yield information on different properties of this barrier, where TEER measures the epithelial permeability to ions at a given point of time while the flux assay, the permeability to molecules over a period of time [42]. It is known that the TJ channels to ions and small molecules are formed by different claudins [36,43] while the flux of large molecules may depend on the occludin junctional content [42,43]. Therefore, these channels can be

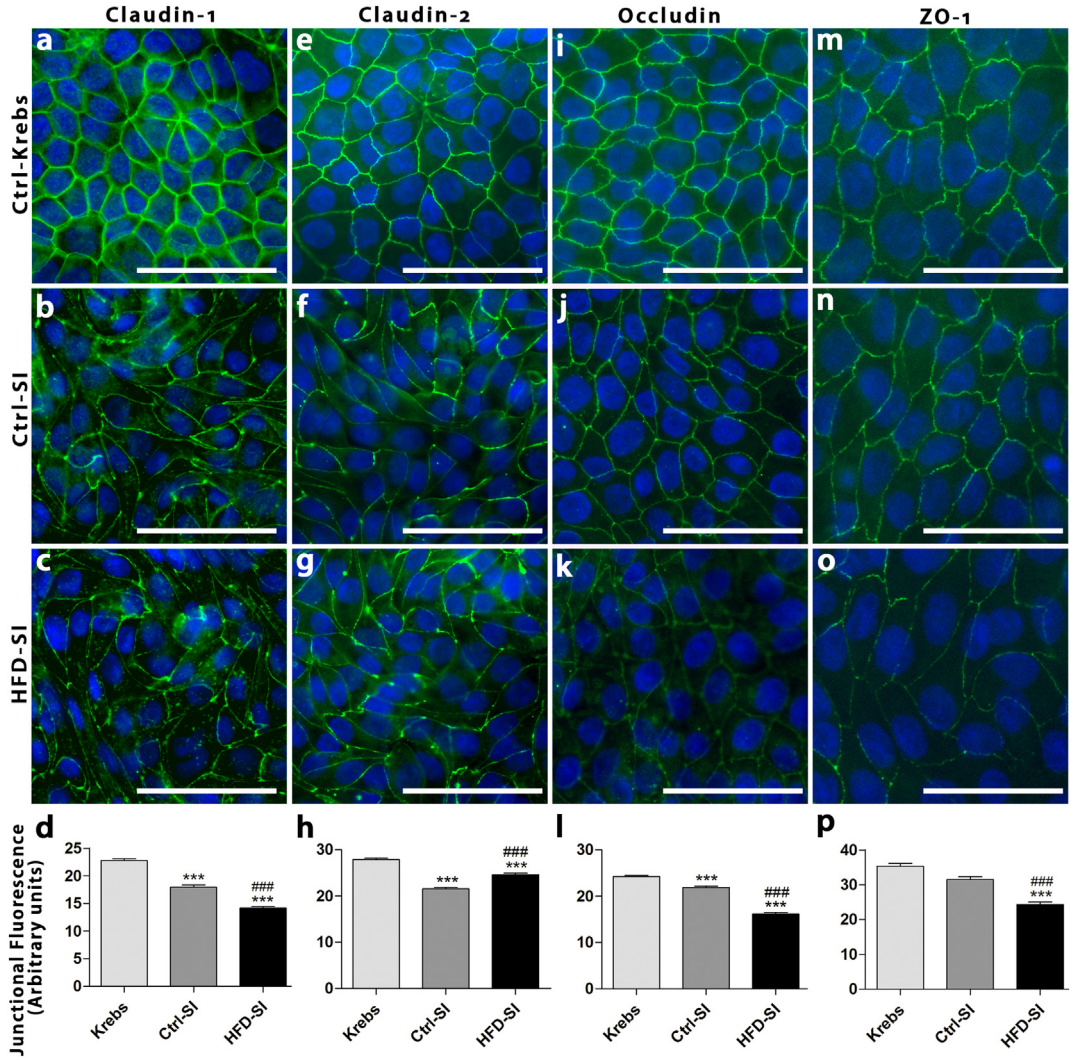

Fig. 6. Intercellular distribution and content of tight junctional proteins in MDCK monolayers after 4 h-exposure to the luminal content of small intestine (SI) isolated from control (Ctrl) and high-fat-fed (HFD) prediabetic mice.

Images a–c, e–g, i–k, m–o display tight junction-associated proteins evaluated by immunofluorescence in MDCK monolayers (claudin-1, claudin-2, occludin, and ZO-1 in green - FITC; DAPI/nuclei in blue). The junctional fluorescence degree analysis at cell-to-cell contact showed a significant decrease in claudin-1 (d), claudin-2 (h), occludin (l), and ZO-1 (p) after 4 h exposure to SI in relation to Krebs (n = 4–6 monolayers/group), which was even greater when exposed to HFD-SI (except for claudin-2) as compared to Ctrl-LI. Scale bar, 50 μm. ***P < 0.0001 in relation to Krebs; ###P < 0.0001 in relation to Ctrl-SI (One-way ANOVA and Bonferroni's post-test). (For interpretation of the references to color in this figure legend, the reader is referred to the web version of this article.)

independently regulated [36]. One possibility is that the increase in transepithelial flux seen herein may be a result, at least in part, of the disruption of the TJ structure (involving junctional proteins associated to the barrier-forming channels, *i.e.* claudin-1, occludin and ZO-1) in conjunction with some cell loss or increase in membrane permeability due to cell death seen after exposure to LI content. Meanwhile, the increase in TEER may be a result of a decreased expression of pore-forming claudins, such as the claudin-2 that was observed in MDCK cells, which would lead to a significant reduction in the number of ion channels within the TJ, overcoming the ion passage through pathways opened by TJ disruption and/or by cell loss/death within the monolayer.

The LI luminal content induced striking changes in the structure of the TJ-mediated barrier, particularly in MDCK cells. HFD-LI exposure induced a significant decrease in the junctional content of occludin and ZO-1 as well as led to a marked cellular redistribution of claudin-1 (from the junctional region to the cytoplasm), that was also seen, at less intensity, in Ctrl-LI-treated MDCK cells. Claudin-1 is known to be constantly recycled in MDCK and Caco-2 cells [44–46]. Inhibition of the endosomal sorting complexes required for protein transport (ESCRT) has been shown to result in similar alterations to that observed in MDCK exposed to LI, *i.e.* accumulation of claudin-1 within the cytoplasm without altering the location of occludin and ZO-1 [44]. As revealed by Western Blot, these changes in immunolocalization of junctional proteins were accompanied by a significant decrease in cellular expression of occludin and claudin-1 and a tendency of decrease in the case of ZO-1 after LI treatment. In contrast, Caco-2 cells displayed only a significant decrease in ZO-1 junctional content after LI-exposure. Taken all together, these alterations in the TJ structure are in accordance with the increase in paracellular permeability that is indicative of disruption of TJ function.

Overall, our data revealed a greater sensitivity of the MDCK cell line, as compared to Caco-2 cells. The former cell line is derived from kidney and usually not exposed to intestinal contents. However, MDCK is extensively employed in epithelial barrier studies, as it displays well-defined cell polarity and fast growth rate, which makes it a viable model for investigating TJ dynamics [29,30,44]. The higher susceptibility seen in MDCK is probably related to its renal origin, therefore,

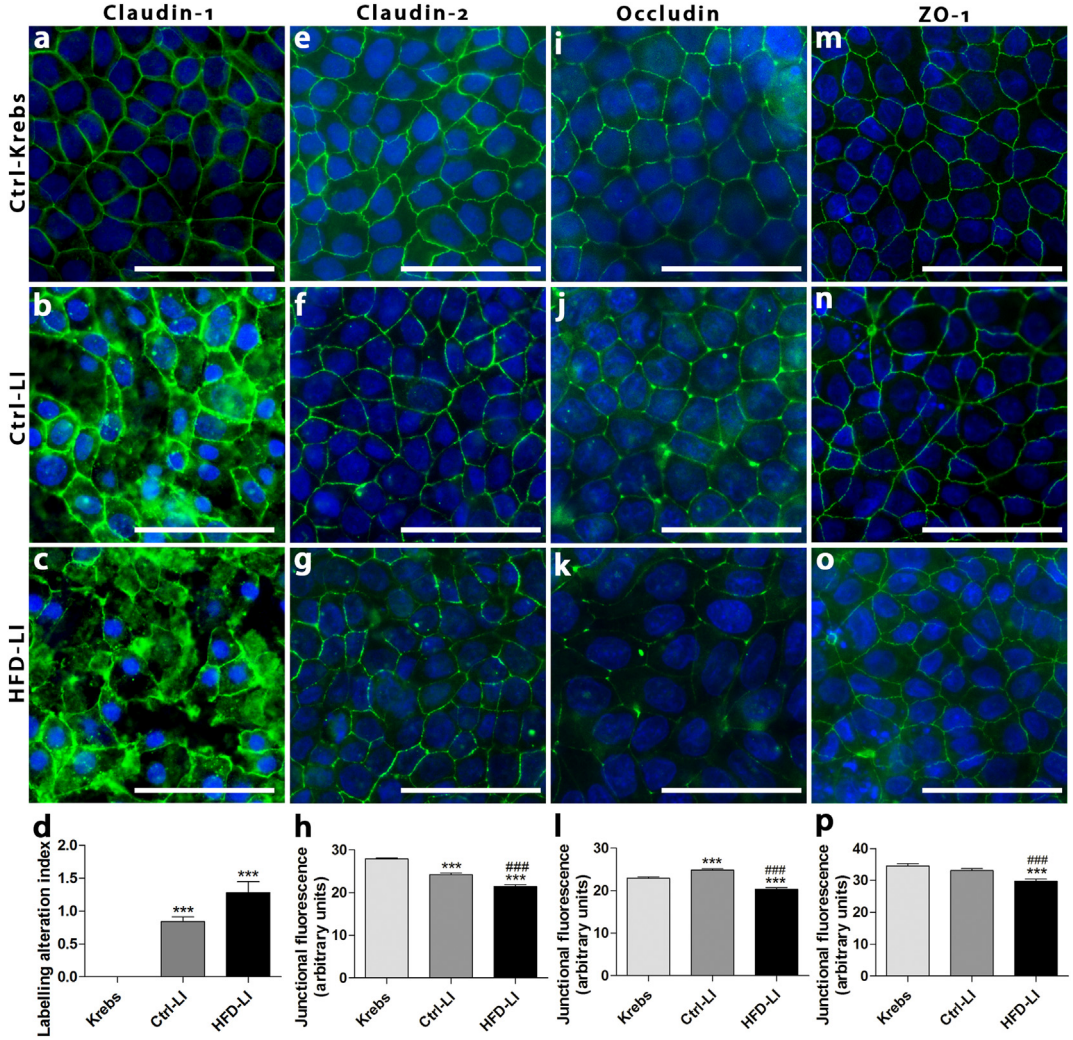

Fig. 7. Intercellular distribution and content of tight junctional proteins in MDCK monolayers after 24 h-exposure to the luminal content of large intestine (LI) isolated from control (Ctrl) and high-fat-fed (HFD) prediabetic mice.

Images a–c, e–g, i–k, m–o display the tight junction-associated proteins evaluated by immunofluorescence in MDCK monolayers (claudin-1, claudin-2, occludin, and ZO-1 in green - FITC; DAPI/nuclei in blue). As seen in images a-c, exposure to Ctrl-LI (b) induced major changes in the intercellular distribution of claudin-1, which were even greater after HFD-Li (c), as confirmed quantitatively (d), as compared to Krebs (a). In addition, HFD-LI induced a decrease in claudin-2 (h), occludin (l), and ZO-1 (p) after 24 h exposure to MDCK monolayers in relation to Krebs and Ctrl-LI (n = 4–6 monolayers/group). Scale bar, 50 μm. ***P < 0.0001 in relation to Krebs; ###P < 0.0001 in relation to Ctrl-SI (One-way ANOVA and Bonferroni's post-test). (For interpretation of the references to color in this figure legend, the reader is referred to the web version of this article.)

not being adapted to intestinal microorganisms and luminal components. Meanwhile, the luminal content of the large intestine, either isolated from normal or prediabetic mice, did not induce marked changes in the Caco-2 cell line, as it did in the case of small luminal content exposure. Such event may be explained by the fact that this cell line originates from a colon adenocarcinoma [28,47], thus displaying intrinsic defense mechanisms against deleterious components found within the LI lumen. In addition, the concentration of short-chain fatty acids (SCFA), which are final fermentation products of nonabsorbable dietary components by the intestinal microbiota [48], is expected to be higher in the large intestine as compared to small intestine because of the relative abundance of microorganisms in the former [49]. SCFA are well known to be one of the most important energy sources of colonocytes, being the butyrate responsible for about 70% of this energy [50,51] and also known to display a significant inhibitory action on the damaging effects of HFD to the intestinal epithelial barrier *in vivo* [26].

The most striking finding of the present study was that the intestinal content isolated from prediabetic mice induced greater alterations to the TJ-mediated epithelial barrier than that obtained from normal mice. The changes in TJ structure described herein, involved a significant reduction in the junctional content of TJ proteins (claudins-1, -2, occludin and ZO-1) that was associated with a decrease in cellular expression in the case of claudins-1, -2, and occludin. TJ is a very dynamic structure and post-translational modifications such as phosphorylation, palmitoylation, and ubiquitination may lead to recycling of TJ proteins (from the junctional region to cytoplasm, and *vice versa*) or to the degradation route [36,44]. Components of the intestinal lumen, mainly those isolated from HFD-fed mice, may activate/inhibit one of these regulatory processes, resulting in the alterations to the TJ structure and function described in our *in vitro* system. Potential candidates of the intestinal lumen that could be accounted for these effects on the epithelial barrier may include the microbial communities (that have been shown to differ among the intestine segments (particularly between small intestine *vs.* large intestine [49,52,53])) or its secreted products/toxins (such as LPS and the serine protease zonulin), as well as proteolytic enzymes of gastric, pancreatic and intestinal origin, and bile acids. All these agents are expected to be modified or increased during diabetes while some of them have been shown to disrupt the epithelial

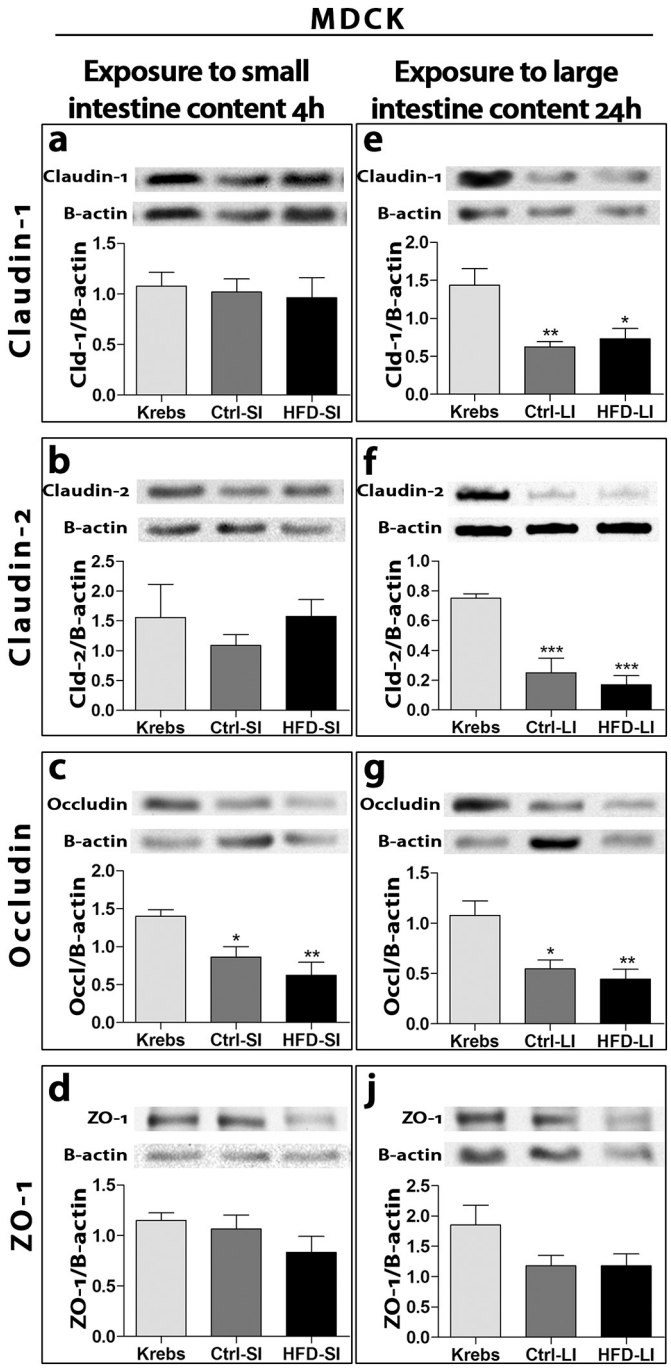

Fig. 8. Immunoblotting for junctional proteins in MDCK monolayers exposed to luminal content of the small intestine (Ctrl-SI; HFD-SI) and large intestine (Ctrl-LI; HFD-LI) isolated from control (Ctrl) and high-fat-fed (HFD) mice.
The optical density analysis of the TJ-associated proteins from MDCK homogenates was performed in membranes obtained by Western Blotting. Exposure to small intestine content for 4 h induced a decrease in occludin (c, n = 8 membranes/group), which was more pronounced after HFD-SI than Ctrl-SI, but no significant change in claudin-1 (a, n = 7–8/group), claudin-2 (b, n = 7–8/group), and ZO-1 (d, n = 8–9/group) cell contents in relation to Krebs-exposed cells. As for the large intestine content, both Ctrl-LI and HFD-LI exposure for 24 h induced a significant decrease in claudin-1 (e, n = 6/group), claudin-2 (f, n = 5/group), and occludin cell contents (g, n = 7/group), in general being even more pronounced after HFD-LI than Ctrl-LI exposure in relation to Krebs. Beta-actin was employed as the loading control. Results are expressed as means ± SEM. *P < 0.05 **P < 0.01 ***P < 0.0001 in relation to Krebs (One-way ANOVA and Bonferroni's post-test).

barrier function *in vitro* and *in vivo* conditions [9,17,23,24,52,54–56].

In conclusion, we demonstrated for the first time that the *in vitro* exposure to the intestine content isolated from HFD-fed prediabetic mice can directly impair the epithelial barrier by affecting the TJ structure/function. This observation suggests that the increased intestinal permeability reported in diabetic rodents and human may involve a direct action of component(s) of the intestinal lumen on the intestinal epithelia. The *in vitro* model proposed in this work can be a useful tool to shed light on the mechanisms underlying the TJ regulation by intestinal microbiota and other components of the intestinal lumen in the context of the T2DM.

Supplementary data to this article can be found online at https://doi.org/10.1016/j.lfs.2018.11.012.

Acknowledgment

The authors thank Dr. Valéria H. A. C. Quitete, Dr. Eduardo Galembeck and Dr. Alexandre L. R. de Oliveira for allowing the access to their laboratory facilities. CBC-B (CNPq# 304991/2015-5) is a recipient of Research Fellowship from Conselho Nacional de Desenvolvimento Científico e Tecnológico (CNPq, Brazil). RBO and LCP were recipients of Ph.D. and MSc. fellowships from CNPq (Brazil), respectively. This work was funded by a grant from Fundação de Amparo à Pesquisa do Estado de São Paulo (FAPESP # 2013/15676-0 and 2018/02118-2, Brazil).

References

[1] World Health Organization, Global Report on Diabetes, http://www.who.int/diabetes/global-Report/En/ (2016), pp. 1–88 (http://www.who.int/about/licensing/%5Cnhttp://apps.who.int/iris/bitstream/10665/204871/1/9789241565257_eng.pdf).
[2] American Diabetes Association, Diagnosis and classification of diabetes mellitus, Diabetes Care 37 (2014) 81–90, https://doi.org/10.2337/dc14-S081.
[3] R.B. Oliveira, C.P.F. Carvalho, C.C. Polo, G.G. Dorighello, C. Boschero, H.C.F. Oliveira, C.B. Collares-Buzato, Impaired compensatory beta-cell function and growth in response to high-fat diet in LDL receptor knockout mice, Int. J. Exp. Pathol. 95 (2014) 296–308, https://doi.org/10.1111/iep.12084.
[4] A. Liston, J.A. Todd, V. Lagou, Beta-cell fragility as a common underlying risk factor in type 1 and type 2 diabetes, Trends Mol. Med. 23 (2017) 181–194, https://doi.org/10.1016/j.molmed.2016.12.005.
[5] D. Tripathy, A.O. Chavez, Defects in insulin secretion and action in the pathogenesis of type 2 diabetes mellitus, Curr. Diab. Rep. 10 (2010) 184–191, https://doi.org/10.1007/s11892-010-0115-5.
[6] R. Burcelin, M. Serino, C. Chabo, V. Blasco-Baque, J. Amar, Gut microbiota and diabetes: from pathogenesis to therapeutic perspective, Acta Diabetol. 48 (2011) 257–273, https://doi.org/10.1007/s00592-011-0333-6.
[7] N. Larsen, F.K. Vogensen, F.W.J. Van Den Berg, D.S. Nielsen, A.S. Andreasen, B.K. Pedersen, W.A. Al-Soud, S.J. Sørensen, L.H. Hansen, M. Jakobsen, Gut microbiota in human adults with type 2 diabetes differs from non-diabetic adults, PLoS One 5 (2010), https://doi.org/10.1371/journal.pone.0009085.
[8] A.P.B. Moreira, T.F.S. Texeira, A.B. Ferreira, M. do Carmo Gouveia Peluzio, R. de Cássia Gonçalves Alfenas, Influence of a high-fat diet on gut microbiota, intestinal permeability and metabolic endotoxaemia, Br. J. Nutr. 108 (2012) 801–809, https://doi.org/10.1017/S0007114512001213.
[9] P.D. Cani, R. Bibiloni, C. Knauf, A.M. Neyrinck, N.M. Delzenne, Changes in gut microbiota control metabolic diet–induced obesity and diabetes in mice, Diabetes 57 (2008) 1470–1481, https://doi.org/10.2337/db07-1403.
[10] P.D. Cani, J. Amar, M.A. Iglesias, M. Poggi, C. Knauf, D. Bastelica, A.M. Neyrinck, F. Fava, K.M. Tuohy, C. Chabo, J. Ferrie, G.R. Gibson, L. Casteilla, N.M. Delzenne, M.C. Alessi, Metabolic endotoxemia initiates obesity and insulin resistance, Diabetes 56 (2007) 1761–1772, https://doi.org/10.2337/db06-1491.P.D.C.
[11] M.M. France, J.R. Turner, The mucosal barrier at a glance, J. Cell Sci. 130 (2017) 307–314, https://doi.org/10.1242/jcs.193482.
[12] S. Amasheh, M. Fromm, D. Günzel, Claudins of intestine and nephron - a correlation of molecular tight junction structure and barrier function, Acta Physiol. 201 (2011) 133–140, https://doi.org/10.1111/j.1748-1716.2010.02148.x.
[13] L. González-Mariscal, A. Betazos, P. Nava, B.E. Jaramill, Tight junction proteins, Prog. Biophys. Mol. Biol. 81 (2003) 1–44, https://doi.org/10.1016/S0079-6107(02)00037-8.
[14] S.F. Assimakopoulos, I. Papageorgiou, A. Charonis, Enterocytes' tight junctions: from molecules to diseases, World J. Gastrointest. Pathophysiol. 6 (2011) 123–137, https://doi.org/10.4291/wjgp.v2.i6.123.
[15] E.Y. Huang, V.A. Leone, S. Devkota, Y. Wang, M.J. Brady, E.B. Chang, Composition of dietary fat source shapes gut microbiota architecture and alters host inflammatory mediators in mouse adipose tissue, J. Parenter. Enter. Nutr. 37 (2013) 746–754, https://doi.org/10.1177/0148607113486931.

[16] C.B. La Serre, C.L. Ellis, J. Lee, A.L. Hartman, J.C. Rutledge, H.E. Raybould, Propensity to high-fat diet-induced obesity in rats is associated with changes in the gut microbiota and gut inflammation propensity to high-fat diet-induced obesity in rats is associated with changes in the gut microbiota and gut inflammation, Am. J. Physiol. Gastrointest. Liver Physiol. 299 (2010) 440–448, https://doi.org/10.1152/ajpgi.00098.2010.
[17] T. Suzuki, H. Hara, Dietary fat and bile juice, but not obesity, are responsible for the increase in small intestinal permeability induced through the suppression of tight junction protein expression in LETO and OLETF rats, Nutr. Metab. 7 (2010) 1–19, https://doi.org/10.1186/1743-7075-7-19.
[18] B.M. Mongelli-Sabino, L.P. Canuto, C.B. Collares-Buzato, Acute and chronic exposure to high levels of glucose modulates tight junction-associated epithelial barrier function in a renal tubular cell line, Life Sci. 188 (2017) 149–157, https://doi.org/10.1016/j.lfs.2017.09.004.
[19] T. Sawai, R.A. Drongowski, R.W. Lampman, A.G. Coran, C.M. Harmon, The effect of phospholipids and fatty acids on tight-junction permeability and bacterial translocation, Pediatr. Surg. Int. 17 (2001) 269–274, https://doi.org/10.1007/s003830100592.
[20] T. Liu, H. Hougen, A.C. Vollmer, S.M. Hiebert, Gut bacteria profiles of *Mus musculus* at the phylum and family levels are influenced by saturation of dietary fatty acids, Anaerobe 18 (2012) 331–337, https://doi.org/10.1016/j.anaerobe.2012.02.004.
[21] V. Patrone, S. Ferrari, M. Lizier, F. Lucchini, A. Minuti, B. Tondelli, E. Trevisi, F. Rossi, M.L. Callegari, Short-term modifications in the distal gut microbiota of weaning mice induced by a high-fat diet, Microbiology 158 (2012) 983–992, https://doi.org/10.1099/mic.0.054247-0.
[22] P.D. Cani, S. Possemiers, T. Van de Wiele, Y. Guiot, A. Everard, O. Rottier, L. Geurts, D. Naslain, A. Neyrinck, D.M. Lambert, G.G. Muccioli, N.M. Delzenne, Changes in gut microbiota control inflammation in obese mice through a mechanism involving GLP-2-driven improvement of gut permeability, Gut 58 (2009) 1091–1103, https://doi.org/10.1136/gut.2008.165886.
[23] A. Fasano, Physiological, pathological, and therapeutic implications of zonulin-mediated intestinal barrier modulation, Am. J. Pathol. 173 (2008) 1243–1252, https://doi.org/10.2353/ajpath.2008.080192.
[24] Q. Ramadan, L. Jing, Characterization of tight junction disruption and immune response modulation in a miniaturized Caco-2/U937 coculture-based in vitro model of the human intestinal barrier, Biomed. Microdevices 18 (2016) 11, https://doi.org/10.1007/s10544-016-0035-5.
[25] L. Wen, A. Duffy, Factors influencing the gut microbiota, inflammation, and type 2 diabetes, J. Nutr. (2017) 1468S–1472S, https://doi.org/10.3945/jn.116.240754.
[26] V. Matheus, L. Monteiro, R. Oliveira, D. Maschio, C. Collares-Buzato, Butyrate reduces high-fat diet-induced metabolic alterations, hepatic steatosis and pancreatic beta cell and intestinal barrier dysfunctions in prediabetic mice, Exp. Biol. Med. (2017), https://doi.org/10.1177/1535370217708188.
[27] R.B. Oliveira, D.A. Maschio, C.P.F. Carvalho, C.B. Collares-Buzato, Influence of gender and time diet exposure on endocrine pancreas remodeling in response to high fat diet-induced metabolic disturbances in mice, Ann. Anat. 200 (2015) 88–97, https://doi.org/10.1016/j.aanat.2015.01.007.
[28] Y. Sambuy, I. De Angelis, G. Ranaldi, M.L. Scarino, A. Stammati, F. Zucco, The Caco-2 cell line as a model of the intestinal barrier: influence of cell and culture-related factors on Caco-2 cell functional characteristics, Cell Biol. Toxicol. 21 (2005) 1–26, https://doi.org/10.1007/s10565-005-0085-6.
[29] J.D. Dukes, P. Whitley, A.D. Chalmers, The MDCK variety pack: choosing the right strain, BMC Cell Biol. 12 (2011) 2–5, https://doi.org/10.1186/1471-2121-12-43.
[30] E.B.M.I. Peixoto, C.B. Collares-Buzato, Protamine-induced epithelial barrier disruption involves rearrangement of cytoskeleton and decreased tight junction-associated protein expression in cultured MDCK strains, Cell Struct. Funct. 29 (2005) 165–178, https://doi.org/10.1247/csf.29.165.
[31] C.B. Collares-Buzato, M.A. Jepson, G.T.A. McEwan, B.H. Hirst, N.L. Simmons, Co-culture of two MDCK strains with distinct junctional protein expression: a model for intercellular junction rearrangement and cell sorting, Cell Tissue Res. 291 (1998) 267–276, https://doi.org/10.1007/s004410050996.
[32] S.D. Hauschka, I.R. Konigsberg, The influence of collagen on the development of muscle clones, Proc. Natl. Acad. Sci. U. S. A. 55 (1966) 119–126, https://doi.org/10.1073/pnas.55.1.119.
[33] S. Sutton, Measurement of microbial cells by optical density, J. Valid. Technol. 17 (2011) 46–49.
[34] M.R.G. Maia, S. Marques, A.R.J. Cabrita, R.J. Wallace, G. Thompson, A.J.M. Fonseca, H.M. Oliveira, Simple and versatile turbidimetric monitoring of bacterial growth in liquid cultures using a customized 3D printed culture tube holder and a miniaturized spectrophotometer: application to facultative and strictly anaerobic bacteria, Front. Microbiol. 7 (2016) 1381, https://doi.org/10.3389/fmicb.2016.01381.
[35] D.A. Maschio, R.B. Oliveira, M.R. Santos, C.P.F. Carvalho, H.C.L. Barbosa-Sampaio, C.B. Collares-Buzato, Activation of the Wnt/β-catenin pathway in pancreatic beta cells during the compensatory islet hyperplasia in prediabetic mice, Biochem. Biophys. Res. Commun. 478 (2016) 1534–1540, https://doi.org/10.1016/j.bbrc.2016/08.146.
[36] D. Gunzel, A.S.L. Yu, Claudins and the modulation of tight junction permeability, Physiol. Rev. 93 (2013) 525–569, https://doi.org/10.1152/physrev.00019.2012.
[37] M. Schumann, B. Siegmund, J.D. Schulzke, M. Fromm, Celiac disease: role of the epithelial barrier, Cell. Mol. Gastroenterol. Hepatol. 3 (2017) 150–162, https://doi.org/10.1016/j.jcmgh.2016.12.006.
[38] M. Gagnon, A. Zihler Berner, N. Chervet, C. Chassard, C. Lacroix, Comparison of the Caco-2, HT-29 and the mucus-secreting HT29-MTX intestinal cell models to investigate *Salmonella* adhesion and invasion, J. Microbiol. Methods 94 (2013) 274–279, https://doi.org/10.1016/j.mimet.2013.06.027.
[39] M. Cohen, X.-Q. Zhang, H.P. Senaati, H.-W. Chen, N.M. Varki, R.T. Schooley, P. Gagneux, Influenza A penetrates host mucus by cleaving sialic acids with neuraminidase, Virol. J. 10 (2013) 321, https://doi.org/10.1186/1743-422X-10-321.
[40] M. Natoli, B.D. Leoni, I. D'Agnano, F. Zucco, A. Felsani, Good Caco-2 cell culture practices, Toxicol. in Vitro 26 (2012) 1243–1246, https://doi.org/10.1016/j.tiv.2012.03.009.
[41] P.D. Ward, D.R. Thakker, Enhancing paracellular permeability by modulating epithelial tight junctions, Pharm. Sci. Technol. Today 3 (2000) 346–358.
[42] M.S. Balda, J.A. Whitney, C. Flores, S. González, M. Cereijido, K. Matter, Functional dissociation of paracellular permeability and transepithelial electrical resistance and disruption of the apical-basolateral intramembrane diffusion barrier by expression of a mutant tight junction membrane protein, J. Cell Biol. 134 (1996) 1031–1049, https://doi.org/10.1083/jcb.134.4.1031.
[43] R. Al-Sadi, K. Khatib, S. Guo, D. Ye, M. Youssef, T. Ma, Occludin regulates macromolecule flux across the intestinal epithelial tight junction barrier, Am. J. Physiol. Gastrointest. Liver Physiol. 300 (2011) G1054–G1064, https://doi.org/10.1152/ajpgi.00055.2011.
[44] J.D. Dukes, L. Fish, J.D. Richardson, E. Blaikley, S. Burns, C.J. Caunt, A.D. Chalmers, P. Whitley, Functional ESCRT machinery is required for constitutive recycling of claudin-1 and maintenance of polarity in vertebrate epithelial cells, Mol. Biol. Cell 22 (2011) 3192–3205, https://doi.org/10.1091/mbc.E11-04-0343.
[45] J.D. Dukes, P. Whitley, A.D. Chalmers, The pikfyve inhibitor YM201636 blocks the continuous recycling of the tight junction proteins claudin-1 and claudin-2 in MDCK cells, PLoS One 7 (2012) 1–10, https://doi.org/10.1371/journal.pone.0028659.
[46] S. Takahashi, N. Iwamoto, H. Sasaki, M. Ohashi, Y. Oda, S. Tsukita, M. Furuse, The E3 ubiquitin ligase LNX1p80 promotes the removal of claudins from tight junctions in MDCK cells, J. Cell Sci. 122 (2009) 985–994, https://doi.org/10.1242/jcs.040055.
[47] M.J. Engle, G.S. Goetz, D.H. Alpers, Caco-2 cells express a combination of colonocyte and enterocyte phenotypes, J. Cell. Physiol. 174 (1998) 362–369, https://doi.org/10.1002/(SICI)1097-4652(199803)174:3<362::AID-JCP10>3.0.CO;2-B.
[48] G.T. Macfarlane, G.R. Gibson, Carbohydrate fermentation, energy transduction and gas metabolism in the human large intestine, in: R.I. Mackie, B.A. White (Eds.), Gastrointest. Microbiol. Springer, Boston, MA, Boston, MA, 1997, pp. 269–318, , https://doi.org/10.1007/978-1-4615-4111-0_9.
[49] S. Gu, D. Chen, J.-N. Zhang, X. Lv, K. Wang, L.-P. Duan, Y. Nie, X.-L. Wu, Bacterial community mapping of the mouse gastrointestinal tract, PLoS One 8 (2013), https://doi.org/10.1371/journal.pone.0074957.
[50] W. Scheppach, Effects of short chain fatty acids on gut morphology and function, Gut 35 (1994) S35–S38, https://doi.org/10.1136/gut.35.1_Suppl.S35.
[51] S.E. Pryde, S.H. Duncan, G.L. Hold, C.S. Stewart, H.J. Flint, The microbiology of butyrate formation in the human colon, FEMS Microbiol. Lett. 217 (2002) 133–139, https://doi.org/10.1111/j.1574-6968.2002.tb11467.x.
[52] R. Wirth, N. Bódi, G. Maróti, M. Bagyánszki, P. Talapka, E. Fekete, Z. Bagi, K.L. Kovács, Regionally distinct alterations in the composition of the gut microbiota in rats with streptozotocin-induced diabetes, PLoS ONE 9 (2014) e110440, , https://doi.org/10.1371/journal.pone.0110440.
[53] D. Li, H. Chen, B. Mao, Q. Yang, J. Zhao, Z. Gu, H. Zhang, Y.Q. Chen, W. Chen, Microbial biogeography and core microbiota of the rat digestive tract, Sci. Rep. 7 (2017) 45840, https://doi.org/10.1038/srep45840.
[54] H. Van Spaendonk, H. Ceuleers, L. Witters, E. Patteet, J. Joossens, K. Augustyns, A.M. Lambeir, I. De Meester, J.G. De Man, B.Y. De Winter, Regulation of intestinal permeability: the role of proteases, World J. Gastroenterol. 23 (2017) 2106–2123, https://doi.org/10.3748/wjg.v23.i12.2106.
[55] L.K. Stenman, R. Holma, R. Korpela, High-fat-induced intestinal permeability dysfunction associated with altered fecal bile acids, World J. Gastroenterol. 18 (2012) 923–929, https://doi.org/10.3748/wjg.v18.i9.923.
[56] C. Sturgeon, A. Fasano, Zonulin, a regulator of epithelial and endothelial barrier functions, and its involvement in chronic inflammatory diseases, Tissue Barriers 21 (2016), https://doi.org/10.1080/21688370.2016.1251384.